


Small-molecule inhibition of TLR8 through stabilization of its resting state

Shuting Zhang^{1-3,7}, Zhenyi Hu^{2,7}, Hiromi Tanji^{4,7}, Shuangshuang Jiang¹, Nabanita Das², Jing Li⁵, Kentaro Sakaniwa⁴, Jin Jin⁶, Yanyan Bian⁶, Umeharu Ohto⁴, Toshiyuki Shimizu^{4*} & Hang Yin^{1,2} *

Endosomal Toll-like receptors (TLR3, TLR7, TLR8, and TLR9) are highly analogous sensors for various viral or bacterial RNA and DNA molecular patterns. Nonetheless, few small molecules can selectively modulate these TLRs. In this manuscript, we identified the first human TLR8-specific small-molecule antagonists via a novel inhibition mechanism. Crystal structures of two distinct TLR8-ligand complexes validated a unique binding site on the protein-protein interface of the TLR8 homodimer. Upon binding to this new site, the small-molecule ligands stabilize the preformed TLR8 dimer in its resting state, preventing activation. As a proof of concept of their therapeutic potential, we have demonstrated that these drug-like inhibitors are able to suppress TLR8-mediated proinflammatory signaling in various cell lines, human primary cells, and patient specimens. These results not only suggest a novel strategy for TLR inhibitor design, but also shed critical mechanistic insight into these clinically important immune receptors.

The innate immune system senses the presence of pathogen-associated molecular patterns (PAMPs) through a wide variety of germ-line-encoded host sensors termed pattern recognition receptors (PRRs)¹. Toll-like receptor (TLR) family proteins are the most studied and best characterized PRRs, and play a crucial role in the initiation of the hosts' immune responses, linking innate immunity and adaptive immunity^{2,3}. Upon PAMP recognition, TLRs recruit a series of adaptor proteins, which trigger the proinflammatory signaling cascades that result in activation of nuclear factor (NF)- κ B and upregulation of inflammatory cytokines and chemokines^{4,5}. This TLR response is crucial for helping to eliminate the pathogen and establishing long lasting adaptive responses, but also can cause various autoimmune diseases and inflammatory disorders⁶⁻⁸.

Ten different TLRs (TLR1 through 10) have been identified in humans, located at both the plasma and the endosome membranes⁹. The endosomal TLRs detect viral and endogenous double-stranded RNA (dsRNA; TLR3), singled-stranded RNA (ssRNA; TLR7/8), or unmethylated CpG sequences in DNA (TLR9) as pathogen or danger-associated signals¹⁰. In humans, TLR7 and TLR8 are phylogenetically and structurally related, sharing little difference in sequence and structure homology. Both TLR7 and TLR8 recognize viral ssRNA, as well as synthetic tricyclic imidazoquinoline derivatives¹¹⁻¹⁴. Despite the essential roles of endosomal TLRs in the induction of the immune response to invading microbial pathogens, inappropriate engagement of these receptors on B cells may initiate and/or perpetuate autoimmune responses and tissue injury¹⁵. There is now considerable emerging evidence indicating that excessive activation of endosomal TLRs substantially contributes to the pathogenesis of a variety of autoimmune diseases^{16,17}. However, only a few small-molecule inhibitors of these endosomal TLRs have been reported in the literature^{18,19}.

In particular, small-molecule inhibitors for TLR8 have not yet been identified, although their potential value as anti-inflammatory therapeutics continues to drive considerable pharmaceutical research and development^{20,21}. This is due in part to protein-RNA complexes typically having expansive, flexible interfaces that are particularly challenging to target with drug-like small molecules. Furthermore, the conventional view has it that PAMP molecules initiate TLR dimerization and trigger proinflammatory signaling cascades, which in turn initiate the signaling cascade^{4,5}. Nonetheless, the TLR8 activation has been suggested to be a more complex, multistep process that first involves the formation of an apo TLR8 dimer after a proteolytic cleavage that subsequently undergoes a conformational change upon ligand binding²²⁻²⁴. Even though there are a number of tricyclic imidazoquinoline compounds reported as TLR8 activators^{25,26}, their direct chemical modifications did not lead to identification of small-molecule inhibitors, indicating that further understanding of the molecular mechanism of TLR8 regulation may be needed^{27,28}.

To discover specific TLR8 signaling inhibitors, we first developed a high-throughput screening (HTS) assay using an in-house engineered HEK-Blue 293 cell line that stably overexpresses human TLR8. With this cell line, we screened a commercial library and identified pyrazolo[1,5-*a*]pyrimidine and 4-phenyl-1-(2*H*)-phthalazinone derivatives as TLR8 inhibitors, sharing little structural similarity with previously reported small-molecule TLR7/8 ligands, which usually have a tricyclic imidazoquinoline scaffold. Further optimization led to a series of highly potent and selective TLR8 inhibitors. These TLR8 inhibitors also demonstrated potent inflammation-suppressing activities in primary peripheral blood mononuclear cells (PBMC), as well as patient specimens from a variety of autoimmune and inflammatory disorders. On-target validation was confirmed using a combination of TLR-overexpressing

¹School of Pharmaceutical Sciences, Center of Basic Molecular Science, Key Laboratory of Bioorganic Phosphorus Chemistry and Chemical Biology (Ministry of Education), Department of Chemistry, Tsinghua University, Beijing, China. ²Department of Chemistry and Biochemistry and BioFrontiers Institute, University of Colorado Boulder, Boulder, Colorado, USA. ³School of Chemistry and Chemical Engineering, Henan Normal University, Xinxiang, China. ⁴Graduate School of Pharmaceutical Sciences, The University of Tokyo, Tokyo, Japan. ⁵Department of Rheumatology and Clinical Immunology, Peking Union Medical College Hospital and Chinese Academy of Medical Sciences, Key Laboratory of Rheumatology and Clinical Immunology (Ministry of Education), Beijing, China. ⁶Department of Orthopedics, Peking Union Medical College Hospital, Beijing, China. ⁷These authors contributed equally to this work. *e-mail: yin_hang@tsinghua.edu.cn or shimizu@mol.f.u-tokyo.ac.jp

cells, immunoblotting, and structure–activity relationship (SAR) studies. Finally, this series of compounds has demonstrated negligible cytotoxicity, suggesting compelling therapeutic potentials.

To obtain molecular insights into the inhibition mechanism, we solved two crystal structures of different TLR8–inhibitor complexes. Surprisingly, these TLR8 inhibitors consistently bind to a previously unknown site that is only presented by the dimeric, resting state of TLR8. Our TLR8 inhibitors not only stabilize the preformed TLR8 dimer, but also prevent further conformational changes that are necessary for TLR8 activation. This could be a potentially paradigm-shifting discovery, as almost all previous efforts of inhibitor development have focused on targeting the activated form of TLRs^{19,29}. Our results demonstrate that a resting state could provide a novel target for TLR inhibitors.

RESULTS

Identification of potent and selective TLR8 inhibitors

To establish a robust HTS assay for TLR8 inhibitors, we first engineered a cell line stably overexpressing the human TLR8, whose activation can be reported by the secreted embryonic alkaline phosphatase (SEAP) assay. TLR8-overexpressing HEK-Blue cells were prepared by lentiviral infection of HEK-Blue Null1 cells that have null or low basal expression of endogenous TLRs. The overexpression and endosomal localization of human TLR8 was confirmed using confocal microscopy (Supplementary Fig. 1). The TLR8-mediated NF- κ B activation can be assessed by measuring the SEAP activity. Using a previously established NF- κ B inhibitor, triptolide³⁰, as the positive control, a Z'-factor of 0.68 was determined, demonstrating that this assay is robust for HTS (Supplementary Fig. 2).

We next screened a 14,400-membered commercial library (Maybridge HitFinder V11) of diverse, drug-like compounds, which led to identification of 72 compounds as 'hits', inhibiting TLR8 signaling by >85% at 4 μ M (Supplementary Table 1). Cytotoxicity testing at 100 μ M further narrowed down these initial hits to 13. Four compounds, SB1723 (1), SEW04865 (2), BTB08278 (3), and BTB08295 (4) (Supplementary Fig. 3), were eventually selected, as they had proven to be specific inhibitors of TLR8 signaling compared to other homologous TLRs. Interestingly, these four compounds present two distinct chemical scaffolds: SB1723 and SEW04865 both share a 7-phenylpyrazolo[1,5-*a*]pyrimidine backbone; BTB08278 and BTB08295 both contain a 4-phenyl-1-(2*H*)-phthalazinone core structure.

To obtain a more potent small-molecule probe for TLR8, we developed a concise synthetic route for the 7-phenylpyrazolo[1,5-*a*]pyrimidine scaffold for optimization (Supplementary Fig. 4). SAR studies led to the identification of CU-CPT8m (5) with an IC₅₀ of 67 \pm 10 nM and negligible cytotoxicity (Fig. 1a; for the representative SAR results and discussion, see Supplementary Table 2; for syntheses and compound characterizations, see Supplementary Note 1). The direct binding of CU-CPT8m to the ectodomain of human TLR8 was confirmed with isothermal titration calorimetry (ITC). The dissociation constant (K_d) value of CU-CPT8m was determined to be 220 nM (Fig. 1b), which is comparable to that of R848 (K_d = 200 nM)²⁴, a previously established, potent, nonselective TLR7/8 activator³¹.

Given that TLR family proteins are homologous membrane receptors, achieving a high degree of selectivity among TLRs is challenging³². To determine whether CU-CPT8m selectively inhibits TLR8 signaling, we tested CU-CPT8m against all human TLRs. At a concentration of 1 μ M, CU-CPT8m did not show significant inhibition of any TLR other than TLR8 in HEK-Blue cells overexpressing each individual TLR (Fig. 1c). These TLR-overexpressing HEK cells (TLR1/2/6, TLR3, TLR4, TLR5, TLR7, and TLR9 HEK-Blue) present distinct ectodomains, but share common downstream effectors. The fact that CU-CPT8m only reduced the proinflammatory response in the TLR8-overexpressing cells strongly supports the theory that CU-CPT8m directly recognizes TLR8 in cells. It is particularly

notable that TLR7 signaling was not affected at concentrations up to 75 μ M (Supplementary Fig. 5). TLR7 and TLR8 are closely related and share many common ligands (for example, R848). CU-CPT8m is the first reported antagonist in literature with the ability to distinguish between TLR8 and TLR7, implying that a novel molecular recognition mechanism is involved.

CU-CPT8m inhibited TLR8-mediated cytokine production

R848-induced TLR8 activation results in increased production of the proinflammatory cytokines such as TNF- α , IL-6 and IL-8 (ref. 33). We next examined the inhibitory effects of CU-CPT8m in various cell lines. First, we investigated the inhibitory effects of CU-CPT8m on the mRNA level of proinflammatory cytokines by quantitative real-time PCR (RT-PCR). As shown in Figure 1d, treatment with 1 μ M CU-CPT8m completely abolished the elevation of TNF- α and IL-8 mRNA levels induced by R848. By contrast, the inactive analog, 6 (Supplementary Table 2), showed negligible inhibition.

We next showed that CU-CPT8m significantly suppressed the protein level of various cytokines. R848 treatment resulted in a significant elevation of TNF- α production, reaching a maximum of approximately ten-fold after 24 h. Figure 1e demonstrates that CU-CPT8m inhibited R848-induced TNF- α production in the differentiated THP-1 monocytes cells in a dose-dependent manner with an IC₅₀ of 90 \pm 10 nM, which is in good agreement with its IC₅₀ value determined in HEK-Blue TLR8 cells. The negative control compound 6 failed to show significant inhibition at 10 μ M.

Having identified potent and selective inhibitors of TLR8 in cultured cell lines, we then investigated whether CU-CPT8m can regulate TLR8 in primary human cells. Peripheral blood mononuclear cells (PBMCs) include lymphocytes (T cells, B cells, and NK cells), monocytes, and dendritic cells expressing various TLRs. TLR7 and TLR8 are both expressed on B cells and monocytes, whereas DC plasmacytoids (DCps) express only TLR7 and immature DCs (DC11c⁺) express only TLR8 (ref. 34). R848 treatment of PBMCs induced TNF- α secretion, which was reversed by CU-CPT8m, but not by 6, in a dose-dependent manner (Fig. 1f). Notably, TNF- α level was not reduced to baseline by CU-CPT8m, presumably because both TLR7 and TLR8 were activated by R848.

Crystal structure of the CU-CPT8m–TLR8 complex

Previously, two ligand-binding sites have been identified for TLR7 and TLR8 (refs. 24,35). In TLR8, Site 1 is the binding site for the RNA degradant uridine and tricyclic imidazoquinoline ligands (Supplementary Fig. 6) such as R848 and CL097, whereas Site 2 is bound by the dinucleotide UG^{22,23}. We determined the high-resolution X-ray crystal structure of the TLR8–CU-CPT8m complex (Fig. 2a). Interestingly, CU-CPT8m is sandwiched between two protomers (TLR8 and TLR8*^{*}; throughout this paper, asterisks are used to indicate the second TLR8 and its residues) and is accommodated in a hydrophobic pocket on the protein–protein interface of TLR8 and TLR8*^{*}. This pocket is only formed in the preformed dimer in the resting state, and is partially filled with several water molecules in the unliganded form (Fig. 2b). CU-CPT8m forms several interactions with TLR8: van der Waals interactions with hydrophobic residues (F261, F346, V378, I403, F405, F494^{*}, A518^{*}, V520^{*}, and Y567^{*}), π - π stacking with Y348 and F495^{*}, and hydrogen bonds with G351 and V520^{*} (Fig. 2b,c). Upon CU-CPT8m binding, large conformational changes of the loop regions of leucine-rich repeat 8 (LRR8) (F261 and N262) and LRR18 (Y567^{*}) are induced to interact with CU-CPT8m (Fig. 2b), whereas the other regions are not significantly changed (Supplementary Fig. 7a–c). Notably, TLR8 utilizes LRR11–13 for both agonist and antagonist binding on one side of the interface, whereas on the other side, LRR17^{*}–18^{*} and LRR15^{*}–16^{*} are used for agonist and antagonist binding, respectively (Fig. 3). Therefore, this new binding site is close to, but distinct from, the Site 1 previously identified for the agonist, implying a unique inhibitory

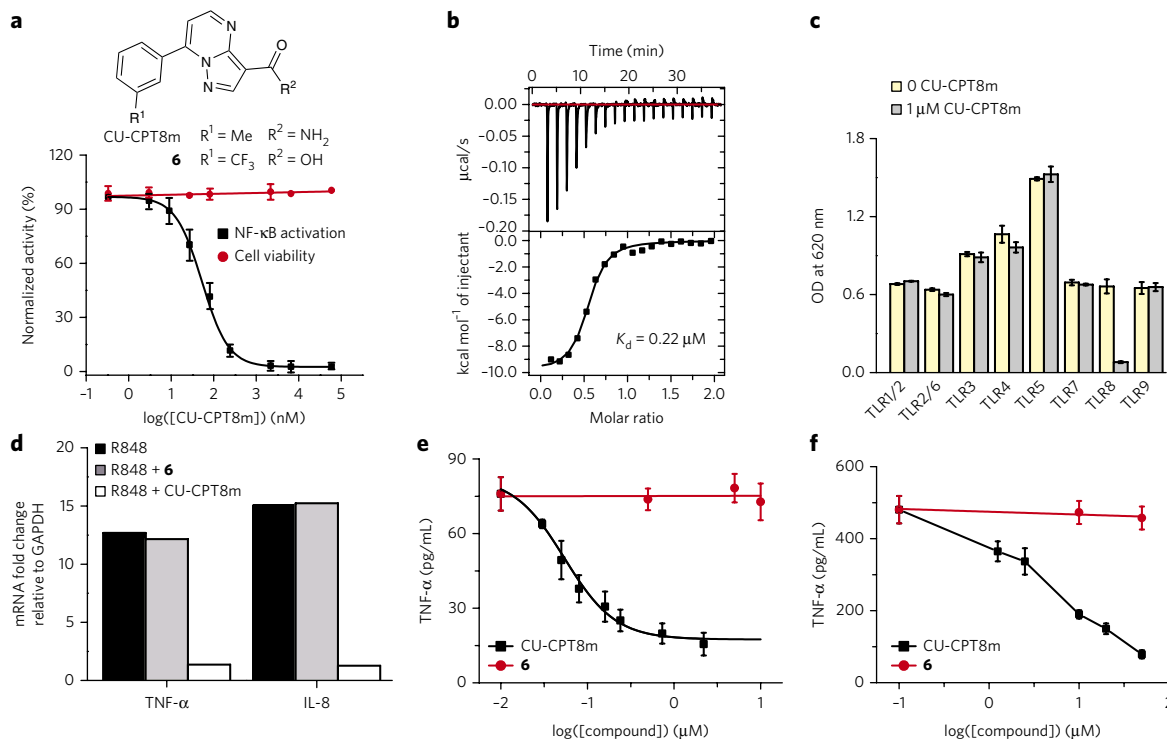


Figure 1 | CU-CPT8m potently and selectively inhibited TLR8. **(a)** Chemical structures of CU-CPT8m and **6** (negative control), and concentration-response curve and dose-dependent cytotoxicity of CU-CPT8m in HEK-Blue TLR8 cell line. Data was normalized to a DMSO control (data are mean \pm s.d.; $n = 3$ independent experiments). **(b)** ITC thermogram of CU-CPT8m titrated into human TLR8 (hTLR8) to determine binding affinity and stoichiometry (representative of one independent experiment). The raw data are presented on top and the integrated peak areas are shown and fitted below. Mean $K_d = 0.22 \mu\text{M}$; stoichiometric binding $N = 0.5$. Red line represents baseline for peak integration. **(c)** Specificity test for CU-CPT8m ($1 \mu\text{M}$) using TLR-specific agonists to selectively activate different HEK-Blue TLR-overexpressing cells in the presence or absence of $1 \mu\text{M}$ CU-CPT8m (data are mean \pm s.d.; $n = 3$ independent experiments). **(d)** TNF- α and IL-8 mRNA levels in R848-treated HEK-Blue TLR8 cells in the presence and absence of $1 \mu\text{M}$ CU-CPT8m or the negative control, **6** ($10 \mu\text{M}$). Data are the average quantification of two independent experiments. **(e)** Dose-dependent response of CU-CPT8m on TLR8-mediated TNF- α production in THP-1 cells with indicated concentrations of CU-CPT8m or **6**. Data are mean \pm s.d.; $n = 3$ independent experiments. **(f)** Dose-dependent response of CU-CPT8m or **6** on TLR8-mediated TNF- α production in PBMC cells induced by $1 \mu\text{g/mL}$ R848. Data are mean \pm s.d.; $n = 3$ independent experiments.

mechanism by CU-CPT8m. In addition, the superimposition of the antagonistic binding sites of TLR7 and TLR8 reveals structural distinctions, which may explain the inhibitory activity of CU-CPT8m specifically against TLR8, but not TLR7, signaling (Supplementary Fig. 7d).

Upon ligand-induced activation, the ectodomains of TLR8 undergo conformational changes, resulting in less separation between their C termini. The distances between the C termini of the two protomers of TLR8 dimer are 49 \AA in TLR8-CU-CPT8m and 51 \AA in the unliganded TLR8 dimer (PDB ID: 3W3G; Figs. 2a and 3). These values are obviously larger than that of agonist-bound activated dimer (34 \AA ; Figs. 2a and 3; TLR8-R848; PDB ID: 3W3N), in which the two C termini come closer to allow dimerization of intracellular domains and downstream signaling²³. Taken together, our findings indicate that CU-CPT8m recognizes a novel binding site on the TLR8-TLR8* interface that is distinct from Site 1 (Fig. 3), whose occupation prevents TLR8 activation.

Inhibition of TLR8 through stabilizing its resting state

Despite CU-CPT8m being potent and selective for TLR8 (Supplementary Fig. 6), the existence of the unutilized residues (for example, S516 and Q519) in the binding pocket suggests that it is possible to further optimize the binding affinity of CU-CPT8m. Therefore, we started another SAR study of 4-phenyl-1-(2H)-phthalazinone, the second, distinct scaffold identified from the HTS, as an alternative seed structure. The structural optimization led to two new picomolar-level TLR8 inhibitors that are structurally

similar to CU-CPT8m: CU-CPT9a (**7**; $\text{IC}_{50} = 0.5 \pm 0.1 \text{ nM}$) and CU-CPT9b (**8**; $\text{IC}_{50} = 0.7 \pm 0.2 \text{ nM}$) (Fig. 4a; for the representative SAR results and discussion, see Supplementary Figs. 8 and 9; Supplementary Table 3). The fact that SARs starting with distinct seeds led to a similar scaffold might imply that such a scaffold is nearly optimal. Accordingly, ITC experiments have confirmed the strong binding of CU-CPT9b with a K_d of 21 nM (Supplementary Fig. 10). These compounds have demonstrated excellent potency in blocking TLR8 activation induced by either R848 or ssRNA (Supplementary Fig. 11), with negligible effects in wild-type HEK 293 cells or in HEK-Blue 293 cells expressing other TLRs.

Next, we carried out on-target validation for CU-CPT9a. The downstream protein levels in cells treated with R848 in the presence or absence of CU-CPT9a were determined using immunoblot analysis (Supplementary Figs. 12 and 17). The p65 component of NF- κ B, phosphorylated IRAK-4 (p-IRAK4), and TRAF3—all downstream to TLR8—showed elevation upon R848 treatment in both THP-1 and HEK-Blue TLR8 cells (data not shown)^{5,36}. This elevation of the downstream protein levels induced by R848 can be reversed by CU-CPT9a in a dose-dependent manner. By contrast, the expression of TRIF and IRF3 (cytoplasmic and nuclear) was only responsive to TLR4 and TLR3 and was independent of TLR8 (refs. 37,38). The expression levels of TRIF and IRF3 did not show significant change in THP-1 cells upon treatment of R848, nor do they change with treatment of CU-CPT9a. Taken together, these immunoblot analysis results support the notion that the inhibitory effects of CU-CPT9a occur specifically through TLR8 in cells.

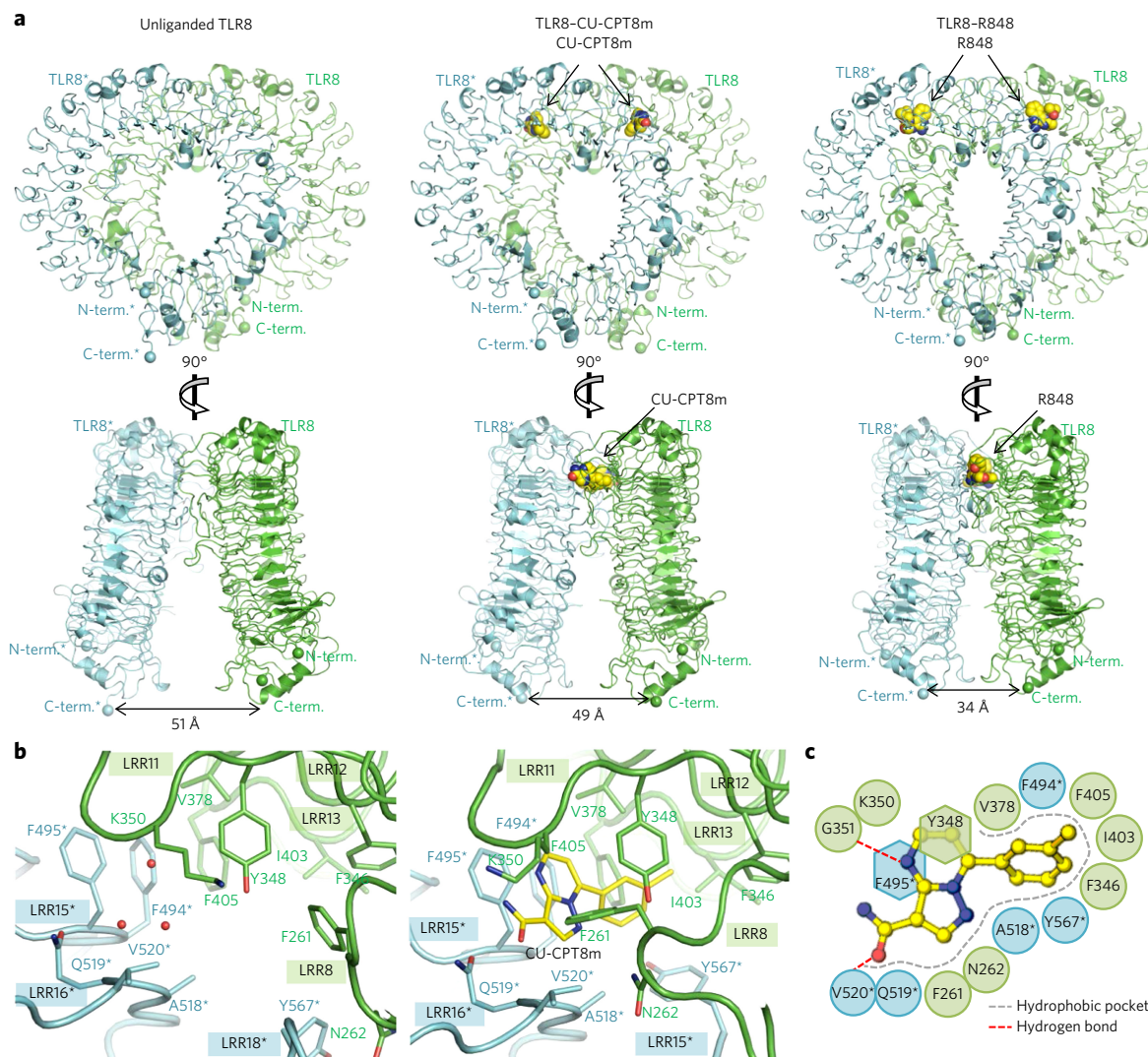


Figure 2 | Crystal structure of the TLR8-CU-CPT8m complex. (a) Front (top) and side (bottom) views of the unliganded (left, PDB ID 3W3G), TLR8-CU-CPT8m (middle) and TLR8-R848 (right, PDB ID 3W3N) complexes. TLR8 and its dimerization partner, TLR8*, are colored green and cyan, respectively. The distances between the C termini of the two protomers of the TLR8 dimer (TLR8-CU-CPT8m) is similar to that of the unliganded dimer (right). Superimposition of the TLR8 structure complexed with CU-CPT8m onto the corresponding unliganded TLR8 segment (residues: 32–816) produces r.m.s. deviation values of 2.4 Å. The ligand molecules are illustrated by space-filling representations. The C, O and N atoms of the ligands are colored yellow, red, and blue, respectively. (b) Close-up view of the antagonist binding site of unliganded TLR8 (left) and TLR8-CU-CPT8m (right). Water molecules are indicated by red filled circles. (c) Schematic representation of interactions between CU-CPT8m and the TLR8 protein. The hydrophobic pocket and hydrogen bonds are shown as dashed gray arcs and dashed red lines, respectively.

To further explore the molecular mechanism of inhibition, we obtained the crystal structure of the TLR8-CU-CPT9b complex. It is shown that CU-CPT9b binds to the inactive TLR8 dimer in a similar way to CU-CPT8m (Fig. 4b). CU-CPT9b utilizes hydrogen bonds with G351 and V520*, which are conserved among TLR8-antagonist structures (Fig. 2c). Additionally, CU-CPT9b forms water-mediated contacts with S516* and Q519* that are not observed in the TLR8-CU-CPT8m structure, suggesting that the enhanced potency of CU-CPT9b derives from the new interactions with these polar residues. The orientation of Y567* also changes to facilitate van der Waals interactions with CU-CPT9b, similar to those of TLR8-CU-CPT8m.

Gel-filtration chromatography with diluted TLR8 proteins, in which TLR8 exists as a monomer, was conducted to determine the dimerization state of TLR8 in the absence and presence of different ligands (Fig. 4c; Supplementary Fig. 13). TLR8 with R848 or CU-CPT9b was shown to elute at a smaller retention volume, which suggested that these ligands bind to TLR8 in a

dose-dependent manner and stabilize the TLR8 dimer in solution. Furthermore, the binding of these CU-CPT derivatives prevented further agonist binding, which was confirmed by ITC experiments (Supplementary Fig. 10).

Collective evidence from CU-CPT8m, CU-CPT9a, and CU-CPT9b demonstrates that this new class of inhibitor binds to TLR8 at a site different from small-molecule agonists (for example, uridine or R848; Fig. 3). Herein we propose a mechanism for these TLR8 inhibitors: upon agonist binding (for example, R848 and uridine with ssRNA), two TLR8 protomers are brought closer to initiate downstream signaling. Binding of the antagonist at the new unique site stabilizes the TLR8 dimer in its resting state, preventing TLR8 from activation (Fig. 3).

Therapeutic potential of small-molecule TLR8 inhibitors

Though previous evidence suggests that TLR8 plays an important role in autoimmune disorders³⁹, the feasibility of targeting these diseases by suppressing TLR8 has not been firmly established. After

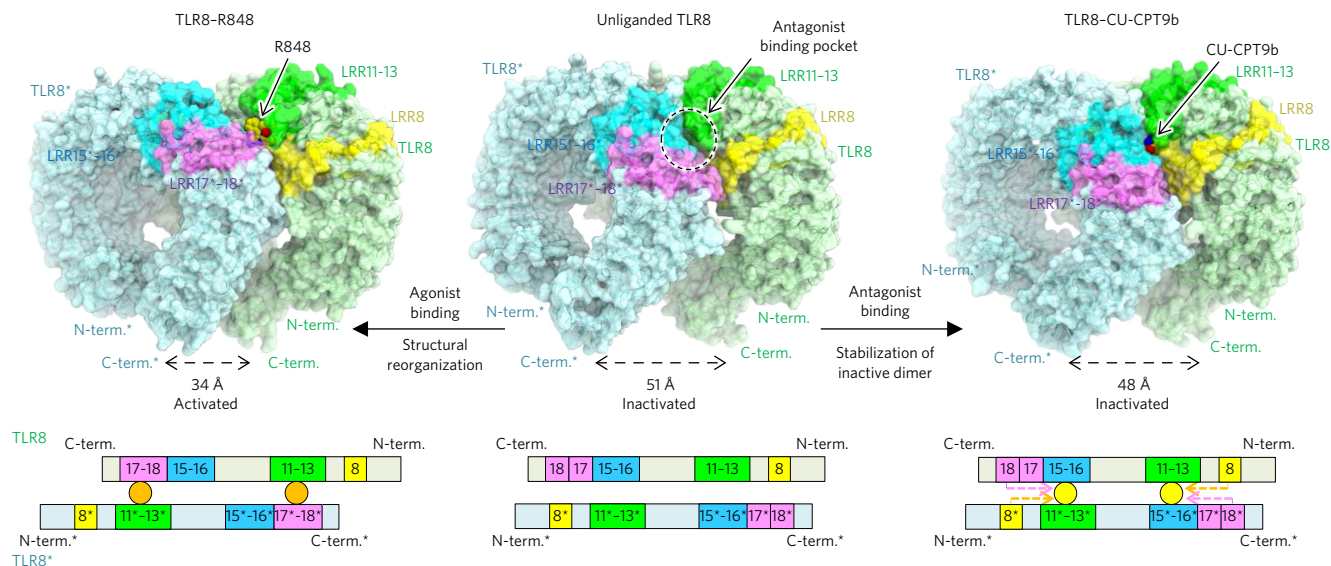


Figure 3 | Proposed antagonistic mechanism of CU-CPT compounds (top) and schematic representation of domain arrangement in each TLR8 forms (bottom). LRR8, LRR11-13, LRR15-16, and LRR17-18 are colored yellow, green, blue, and purple, respectively. In the bottom panel, the antagonist and agonist are illustrated by yellow and orange circles. Interactions between ligands and protruding loop regions are shown by dashed arrows. TLR8 used LRR11-13 in common for both agonist and antagonist binding on one side of the interface, but LRR17^{*}-18^{*} and LRR15^{*}-16^{*} on the other side for agonist and antagonist binding, respectively. Binding of an agonist (for example, R848) brings two TLR8 C termini to a closer distance to initiate downstream signaling, whereas binding of antagonists (for example, CU-CPT8m or CU-CPT9b) at the antagonist binding site stabilizes the inactive TLR8 dimer with C termini further apart, preventing TLR8 activation.

identifying highly potent and selective TLR8 inhibitors, we aimed to validate their therapeutic potential using a more pathologically relevant system. Nonetheless, there is a lack of an appropriate

rodent animal model because TLR8 has been reported as nonfunctional in either mice or rats^{14,31,40}. Therefore, we chose to test these TLR8 inhibitors in human specimens harvested from patients with

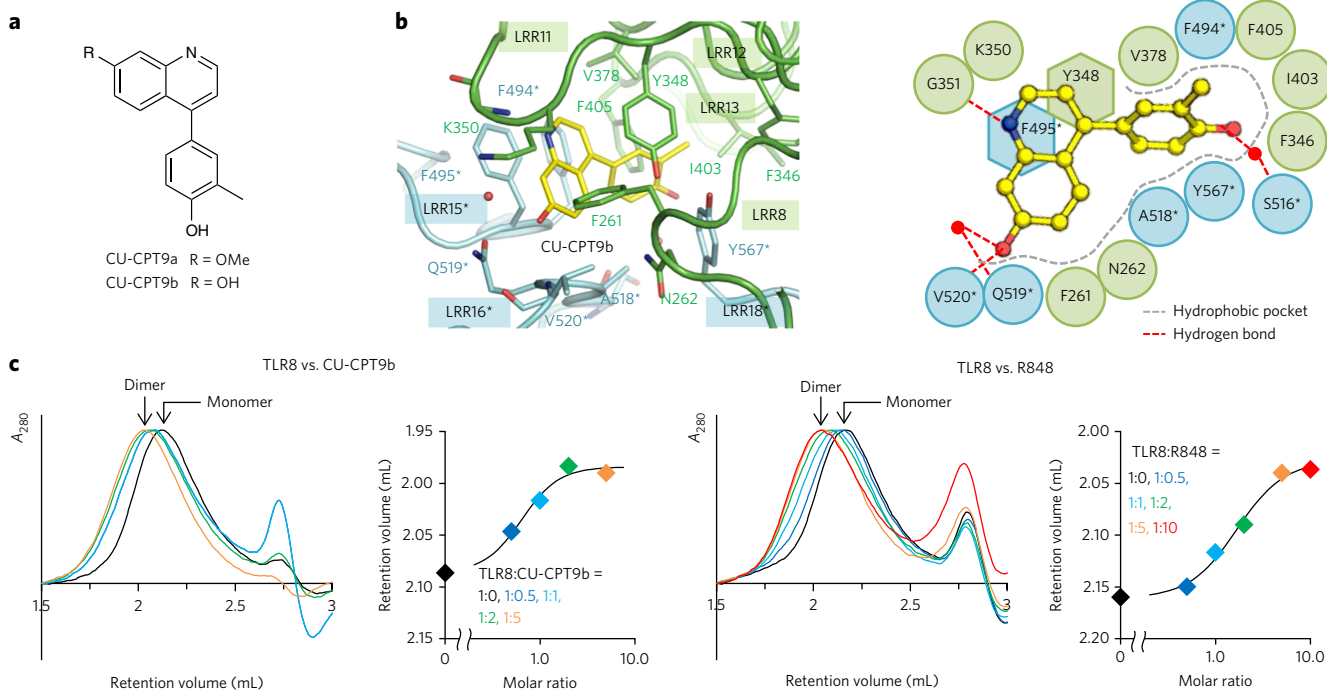


Figure 4 | TLR8 inhibitors consistently recognize an allosteric pocket on the protein-protein interface, stabilizing the inactive TLR8 dimer. (a) Chemical structure of CU-CPT9a and CU-CPT9b. (b) Close-up view of the antagonist binding site (left) and a schematic representation of TLR8-CU-CPT9b (right). The C, O, and N atoms of the ligands are colored yellow, red, and blue, respectively. Water molecules mediating the ligand recognition are indicated by red filled circles and hydrogen bonds by dashed lines. (c) Dose-dependent dimerization of TLR8. Elution profiles of gel-filtration chromatography of TLR8 with CU-CPT9b (left) and R848 (right) at various concentrations. Retention volume and normalized absorbance at 280 nm (A_{280}) are shown on the left, and retention volume of TLR8 peak is plotted against its molar ratio (ligand/TLR8) on the right (representative of one independent experiment).

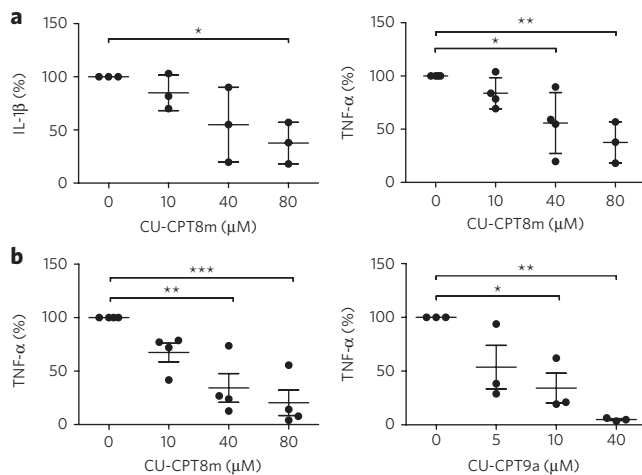


Figure 5 | TLR8 inhibitors suppress the proinflammatory cytokine production in multiple human primary cells derived from different patients. (a) Effect of CU-CPT8m treatment on the production of IL-1 β and TNF- α in synovial cells harvested from osteoarthritis patients. The graph represents percent change 24 h after inhibitor treatment as compared to untreated cells from the same patient. Each data point represents an independent sample read. Center lines indicate means, and whiskers indicate \pm s.d. ($n = 3$ independent experiments for IL-1 β and $n = 4$ independent experiment for TNF- α ; P values were determined using one-way ANOVA; * $P < 0.05$; ** $P < 0.01$). **(b)** Effects of CU-CPT8m and CU-CPT9a treatment on the production of TNF- α in PBMC cells harvested from rheumatoid arthritis patients. Each data point represents an independent sample read. Center lines indicate means, and whiskers indicate \pm s.e.m. ($n = 4$ independent experiments for CU-CPT8m, and $n = 3$ independent experiments for CU-CPT9a; P values were determined using one-way ANOVA; * $P < 0.05$; ** $P < 0.01$; *** $P < 0.001$).

osteoarthritis (OA), rheumatoid arthritis (RA), and adult-onset Still's disease (AOSD). It is well established that TNF- α and IL-1 β are key cytokines in the process of chronic joint inflammation in cartilage. We isolated the synovial cells from synovial tissue of patients who underwent joint replacement surgery because of severe OA. Previous studies have indicated that these pathological tissues express both TLR7 and TLR8 with elevated production of various cytokines, which contributes to extensive articular destruction and functional decline^{41,42}. CU-CPT8m showed significant inhibitory effects in suppressing the spontaneous release of TNF- α and IL-1 β from synovial membrane cultures (Fig. 5a,b) with little cytotoxicity up to 100 μ M (Supplementary Fig. 14). In parallel, we also tested whether CU-CPT8m and CU-CPT9a could reduce the cytokine elevation in PMBCs derived from four patients with RA and one with AOSD, a rare systemic inflammatory disease characterized by the classic triad of persistent high spiking fevers, joint pain, and a distinctive salmon-colored bumpy rash⁴³. CU-CPT8m and CU-CPT9a both significantly suppressed the TNF- α level in a dose-dependent manner (Fig. 5b; Supplementary Fig. 15), which is in agreement with previous reports of TLR8 involvement in these autoimmune diseases³⁹. The negative control compound **6** did not show significant inhibition up to 80 μ M (Supplementary Fig. 16). Although the inhibition of cytokine production by these inhibitors does not necessarily indicate a role for TLR8 in the pathogenesis of these diseases, our results suggest a novel potential therapeutic development strategy for patients' symptom relief.

DISCUSSION

TLRs are homologous PAMP and danger-associated molecular pattern (DAMP) sensors in the innate immune system^{44,45}. However, TLR activation is a double-edged sword: their proinflammatory response

is critical for host defense; nonetheless, excessive TLR activation may lead to the pathogenesis of inflammatory and autoimmune diseases. TLR8, in particular, has been suggested to play substantial roles in various inflammatory disorders and autoimmune diseases. Despite this, very little progress has been made toward the development of drug-like small-molecule inhibitors targeting TLR8.

To discover specific TLR8 signaling inhibitors, we first developed a cell-based, high-throughput screening assay with an engineered HEK-Blue 293 cell line overexpressing human TLR8 and identified compounds bearing pyrazolo[1,5-*a*]pyrimidine and 4-phenyl-1-(2*H*)-phthalazinone core structures as 'hit' inhibitors for TLR8 signaling. With hit-to-lead SAR efforts, we successfully identified highly potent TLR8 inhibitors with \sim 10 μ M IC_{50} values. These compounds efficiently reduced TLR8-mediated NF- κ B activation in various cultured cells (HEK-Blue TLR8 and THP-1) and primary human PBMCs without impairing the responses of other TLRs.

At least part of the lack of TLR8 inhibitors is a result of the poor understanding of the TLR8 activation mechanism. Even though the development of TLR modulators has been an active research field, almost all previous efforts have focused on the recognition of the activated form of TLRs. Unlike other TLRs that require ligand binding for dimerization, TLR8 has been reported to exist in dimeric form before ligand recognition^{23,24}. The recognition of Site 1 and Site 2 by ligands then drives further conformational changes in the ectodomain, leading to dimerization of the TIR domain and initiation of downstream signaling^{23,24}. With the chemical probes newly obtained, we investigated their inhibition mechanism. A striking result is that these inhibitors can stabilize the inactive state of TLR8 by recognizing a distinct pocket from Site 1. By blocking the newly identified site, these TLR8 inhibitors appear to not only stabilize preformed TLR8 dimers, but also antagonize binding of TLR8 activators such as R848 and uridine. Furthermore, this stabilizing of the resting state of TLR dimer subsequently prevents TLR8 from undergoing the conformational change that is necessary for activation. This unconventional modality of regulation by the stabilization of inactive states with allosteric modulators, if confirmed by further works on the dynamics of the dimeric proteins, may be an effective strategy to target other TLR family members (TLR5, 8, and 9) that exist in dimeric form before ligand binding. Finally, we demonstrated the therapeutic potential of these small-molecule TLR8 inhibitors. We explored the effects of CU-CPT8m and CU-CPT9a in human specimens extracted from various inflammation disorders and autoimmune disease patients. Results of this proof-of-concept study showed that CU-CPT9a treatment exerts potent anti-inflammatory effects in the specimens of OA, RA, and AOSD patients, lending further support to previous speculations that TLR8 might play a role in these inflammatory disorder and autoimmune diseases^{7,46}. These studies demonstrated that these TLR8 inhibitors could be used as chemical probes to understand the biological relevance of TLR8 in different pathogenesis processes, and present considerable therapeutic development potential.

Received 5 January 2017; accepted 10 October 2017; published online 20 November 2017

METHODS

Methods, including statements of data availability and any associated accession codes and references, are available in the [online version of the paper](#).

References

- Mogensen, T.H. Pathogen recognition and inflammatory signaling in innate immune defenses. *Clin. Microbiol. Rev.* **22**, 240–273 (2009).
- Broz, P. & Monack, D.M. Newly described pattern recognition receptors team up against intracellular pathogens. *Nat. Rev. Immunol.* **13**, 551–565 (2013).
- Pasare, C. & Medzhitov, R. Toll-like receptors: linking innate and adaptive immunity. *Microbes Infect.* **6**, 1382–1387 (2004).

4. Akira, S., Uematsu, S. & Takeuchi, O. Pathogen recognition and innate immunity. *Cell* **124**, 783–801 (2006).
5. Kawai, T. & Akira, S. Signaling to NF- κ B by Toll-like receptors. *Trends Mol. Med.* **13**, 460–469 (2007).
6. Carpenter, S. & O'Neill, L.A. How important are Toll-like receptors for antimicrobial responses? *Cell. Microbiol.* **9**, 1891–1901 (2007).
7. Kanzler, H., Barrat, F.J., Hessel, E.M. & Coffman, R.L. Therapeutic targeting of innate immunity with Toll-like receptor agonists and antagonists. *Nat. Med.* **13**, 552–559 (2007).
8. Mohammad Hosseini, A., Majidi, J., Baradaran, B. & Yousefi, M. Toll-like receptors in the pathogenesis of autoimmune diseases. *Adv. Pharm. Bull.* **5** Suppl 1: 605–614 (2015).
9. Akira, S. & Takeda, K. Toll-like receptor signalling. *Nat. Rev. Immunol.* **4**, 499–511 (2004).
10. Panter, G., Kuznik, A. & Jerala, R. Therapeutic applications of nucleic acids as ligands for Toll-like receptors. *Curr. Opin. Mol. Ther.* **11**, 133–145 (2009).
11. Gantier, M.P. *et al.* TLR7 is involved in sequence-specific sensing of single-stranded RNAs in human macrophages. *J. Immunol.* **180**, 2117–2124 (2008).
12. Gorden, K.B. *et al.* Synthetic TLR agonists reveal functional differences between human TLR7 and TLR8. *J. Immunol.* **174**, 1259–1268 (2005).
13. Heil, F. *et al.* Species-specific recognition of single-stranded RNA via toll-like receptor 7 and 8. *Science* **303**, 1526–1529 (2004).
14. Hemmi, H. *et al.* Small anti-viral compounds activate immune cells via the TLR7 MyD88-dependent signaling pathway. *Nat. Immunol.* **3**, 196–200 (2002).
15. Papadimitraki, E.D., Bertias, G.K. & Boumpas, D.T. Toll like receptors and autoimmunity: a critical appraisal. *J. Autoimmun.* **29**, 310–318 (2007).
16. Barrat, F.J. *et al.* Nucleic acids of mammalian origin can act as endogenous ligands for Toll-like receptors and may promote systemic lupus erythematosus. *J. Exp. Med.* **202**, 1131–1139 (2005).
17. Marshak-Rothstein, A. Toll-like receptors in systemic autoimmune disease. *Nat. Rev. Immunol.* **6**, 823–835 (2006).
18. Watanabe, M. *et al.* Dihydropyrido[2,3-d]pyrimidines: selective toll-like receptor 9 antagonists from scaffold morphing efforts. *ACS Med. Chem. Lett.* **5**, 1235–1239 (2014).
19. Cheng, K., Wang, X. & Yin, H. Small-molecule inhibitors of the TLR3/dsRNA complex. *J. Am. Chem. Soc.* **133**, 3764–3767 (2011).
20. Hennessy, E.J., Parker, A.E. & O'Neill, L.A. Targeting Toll-like receptors: emerging therapeutics? *Nat. Rev. Drug Discov.* **9**, 293–307 (2010).
21. Kondo, T., Kawai, T. & Akira, S. Dissecting negative regulation of Toll-like receptor signaling. *Trends Immunol.* **33**, 449–458 (2012).
22. Botos, I., Segal, D.M. & Davies, D.R. The structural biology of Toll-like receptors. *Structure* **19**, 447–459 (2011).
23. Tanji, H., Ohto, U., Shibata, T., Miyake, K. & Shimizu, T. Structural reorganization of the Toll-like receptor 8 dimer induced by agonistic ligands. *Science* **339**, 1426–1429 (2013).
24. Tanji, H. *et al.* Toll-like receptor 8 senses degradation products of single-stranded RNA. *Nat. Struct. Mol. Biol.* **22**, 109–115 (2015).
25. Kokatla, H.P. *et al.* Exquisite selectivity for human toll-like receptor 8 in substituted furo[2,3-c]quinolines. *J. Med. Chem.* **56**, 6871–6885 (2013).
26. Salunke, D.B. *et al.* Structure-activity relationships in human Toll-like receptor 8-active 2,3-diamino-furo[2,3-c]pyridines. *J. Med. Chem.* **55**, 8137–8151 (2012).
27. Kuznik, A. *et al.* Mechanism of endosomal TLR inhibition by antimalarial drugs and imidazoquinolines. *J. Immunol.* **186**, 4794–4804 (2011).
28. Schön, M.P. & Schön, M. TLR7 and TLR8 as targets in cancer therapy. *Oncogene* **27**, 190–199 (2008).
29. Lamphier, M. *et al.* Novel small molecule inhibitors of TLR7 and TLR9: mechanism of action and efficacy *in vivo*. *Mol. Pharmacol.* **85**, 429–440 (2014).
30. Liu, H., Liu, Z.H., Chen, Z.H., Yang, J.W. & Li, L.S. Triptolide: a potent inhibitor of NF- κ B in T-lymphocytes. *Acta Pharmacol. Sin.* **21**, 782–786 (2000).
31. Jurk, M. *et al.* Human TLR7 or TLR8 independently confer responsiveness to the antiviral compound R-848. *Nat. Immunol.* **3**, 499 (2002).
32. Yin, H. & Flynn, A.D. Drugging membrane protein interactions. *Annu. Rev. Biomed. Eng.* **18**, 51–76 (2016).
33. Beesu, M. *et al.* Structure-based design of human TLR8-specific agonists with augmented potency and adjuvanticity. *J. Med. Chem.* **58**, 7833–7849 (2015).
34. Valencia Pacheco, G.J. *et al.* Expression and activation of intracellular receptors TLR7, TLR8 and TLR9 in peripheral blood monocytes from HIV-infected patients. *Colomb. Med.* **44**, 92–99 (2013).
35. Zhang, Z. *et al.* Structural analysis reveals that toll-like receptor 7 is a dual receptor for guanosine and single-stranded RNA. *Immunity* **45**, 737–748 (2016).
36. Kaczanowska, S., Joseph, A.M. & Davila, E. TLR agonists: our best frenemy in cancer immunotherapy. *J. Leukoc. Biol.* **93**, 847–863 (2013).
37. Doyle, S. *et al.* IRF3 mediates a TLR3/TLR4-specific antiviral gene program. *Immunity* **17**, 251–263 (2002).
38. Tseng, P.H. *et al.* Different modes of ubiquitination of the adaptor TRAF3 selectively activate the expression of type I interferons and proinflammatory cytokines. *Nat. Immunol.* **11**, 70–75 (2010).
39. Duffy, L. & O'Reilly, S.C. Toll-like receptors in the pathogenesis of autoimmune diseases: recent and emerging translational developments. *ImmunoTargets Ther.* **5**, 69–80 (2016).
40. Liu, J. *et al.* A five-amino-acid motif in the undefined region of the TLR8 ectodomain is required for species-specific ligand recognition. *Mol. Immunol.* **47**, 1083–1090 (2010).
41. Mullen, L., Ferdjani, J. & Sacre, S. Simvastatin inhibits Toll-like receptor 8 (TLR8) signaling in primary human monocytes and spontaneous tumor necrosis factor production from rheumatoid synovial membrane cultures. *Mol. Med.* **21**, 726–734 (2015).
42. Sacre, S.M. *et al.* Inhibitors of TLR8 reduce TNF production from human rheumatoid synovial membrane cultures. *J. Immunol.* **181**, 8002–8009 (2008).
43. Castañeda, S., Blanco, R. & González-Gay, M.A. Adult-onset Still's disease: advances in the treatment. *Best Pract. Res. Clin. Rheumatol.* **30**, 222–238 (2016).
44. Medzhitov, R. Toll-like receptors and innate immunity. *Nat. Rev. Immunol.* **1**, 135–145 (2001).
45. Piccinini, A.M. & Midwood, K.S. DAMPening inflammation by modulating TLR signalling. *Mediators Inflamm.* **2010**, 672395 (2010).
46. Guiducci, C. *et al.* RNA recognition by human TLR8 can lead to autoimmune inflammation. *J. Exp. Med.* **210**, 2903–2919 (2013).

Acknowledgments

This work was funded by the National Institute of Health (NIH R01GM101279 to H.Y.), National Natural Science Foundation of China (No. 21572114 to H.Y. and No. 81401333 to J.L.), the University Key Scientific Research Program Foundation of Henan Province (No. 5201039140120 to S.Z.) and Grant-in-Aid from the Japanese Ministry of Education, Culture, Sports, Science, and Technology (H.T., U.O., and T.S.), CREST JST (T.S.), the Takeda Science Foundation (U.O. and T.S.), the Mochida Memorial Foundation for Medical and Pharmaceutical Research (U.O.), the Naito Foundation (U.O.), and the Daiichi Sankyo Foundation of Life Science (U.O.). We thank X. Wang and W. Wang for their assistance with high-throughput screening and data analysis. We thank J. Dragavon for his assistance with confocal microscopy. We thank Y. Yamada and A. Shinoda for automated data collection at Photon Factory.

Author contributions

H.Y. designed the project and supervised data analysis. S.Z. designed the experiments in consultation with H.Y. S.Z. performed the cell line establishment and high throughput screening. S.Z. and Z.H. performed chemical synthesis of compounds, cell culture and cellular inhibition studies. S.Z., Z.H., S.J., and N.D. performed immunoblotting experiments. H.T., K.S., U.O., and T.S. expressed protein, solved the crystal structure, performed isothermal titration calorimetry and gel-filtration experiments. J.L., J.J., and Y.B. contributed to the patient PBMC and synovial tissues extraction. S.J. performed PBMC and synovial cells extraction. S.J. and S.Z. performed primary cell and patient specimen studies. H.Y. and S.Z. wrote the manuscript with input from Z.H., S.J., and H.T.

Competing financial interests

The authors declare competing financial interests: details accompany the [online version of the paper](#).

Additional information

Any supplementary information, chemical compound information and source data are available in the [online version of the paper](#). Reprints and permissions information is available online at <http://www.nature.com/reprints/index.html>. Publisher's note: Springer Nature remains neutral with regard to jurisdictional claims in published maps and institutional affiliations. Correspondence and requests for materials should be addressed to T.S. or H.Y.

ONLINE METHODS

Cell culture. THP-1 cells were sourced from ATCC and were not further authenticated. The human embryonic kidney (HEK)-Blue Null1, TLR2-, TLR4-, TLR7-, and TLR9-overexpressing HEK-Blue cells were purchased (InvivoGen) and were not further authenticated. Stable TLR3- and TLR5- overexpressing HEK-Blue cells were generated by lentiviral infection of HEK-Blue Null1 cells and functionally authenticated in our laboratory as previously described^{47–49}. The stable TLR8-overexpressing HEK-Blue cells were authenticated by confocal microscopy and functional validation (**Supplementary Figs. 1 and 2**). All cultured cells were grown at 37 °C in a humidified incubator containing 5% CO₂. HEK-Blue TLR cells were cultured in complete culture medium: Dulbecco's modified Eagle's medium (DMEM), 10% (v/v) FBS, 50 U/mL penicillin, 50 mg/mL streptomycin, 100 mg/mL normocin, and 2 mM L-glutamine. THP-1 were cultured in Roswell Park Memorial Institute (RPMI) 1640 medium supplemented with 10% (v/v) FBS, 2 mM L-glutamine, 100 µg/mL streptomycin and 100 U/mL penicillin and 0.05 mM 2-mercaptoethanol. The cultures were checked periodically and found to be free of mycoplasma contamination.

Confocal imaging. Cells were fixed using a 4% (w/v) solution of paraformaldehyde made up in PBS and incubated for 10 min at 20 °C. Following fixation, cells were made permeable with 0.2% (v/v) Triton X-100 made up in PBS at 20 °C. TLR8 antibody (Novus Biologicals; NBP2-24972) was added in PBS containing 1% FBS, then incubated for 10 min. Cell nuclei were stained with 0.2 µg/mL Hoechst 33342 (Thermo Fisher Scientific) in PBS for 10 min, and plasma membrane was stained with CellMask Orange Plasma Membrane Stain (Thermo Fisher Scientific) for 10 min. Cells were imaged on a Nikon Spinning Disc Confocal microscope. All images were captured using a ×100 objective.

SEAP reporter assay. HEK-Blue TLR8 cells were plated at 3.5×10^5 cells/mL in a tissue culture treated 96-well plate in DMEM with 10% (v/v) FBS (deactivated phosphatases). Then cells were treated with 1 µg/mL R848 (Invivogen) and varying concentrations of appropriate compounds. Cells were incubated with compounds and R848 at 37 °C. After 20–24 h of incubation, 20 µL of culture media was removed and placed in a new 96-well plate. 180 µL of Quanti-Blue (Invivogen) was added to the media, and the plate was incubated at 37 °C until color change was observed (30 min to 1 h). Plates were then quantified on a Beckman-Coulter DTX 880 Multimode Detector by measuring absorbance at 620 nm. Data was normalized as readout of ligand-treated cells is 100% activation and untreated cells are 0% activation.

Toll-like receptor (TLR) selectivity assay. The selectivity of compounds against the TLR family was examined in HEK-Blue cells overexpressing a specific TLR and accessory proteins. The assay was performed in the same manner as “SEAP reporter assay,” except that polyriboinosinic:polyribocytidylic acid (poly(I:C)) (5 µg/mL), LPS (lipopolysaccharide) (20 ng/mL), Pam3CSK4 (*N*-palmitoyl-*S*-[2,3-bis(palmitoyloxy)-(2*RS*)-propyl]-[*R*]-cysteiny]-[*S*]-seryl]-[*S*]-lysyl]-[*S*]-lysyl]-[*S*]-lysyl]-[*S*]-lysine3HCl) (100 ng/mL), Pam2CSK4 (*S*-[2,3-bis(palmitoyloxy)-(2*RS*)-propyl]-[*R*]-cysteiny]-[*S*]-seryl]-[*S*]-lysyl]-[*S*]-lysyl]-[*S*]-lysyl]-[*S*]-lysine3CF₃COOH) (100 ng/mL), Flagellin (50 ng/mL), R848 (1 µg/mL), and ODN2006 (0.15 µM) were used to selectively activate HEK-Blue hTLR3, hTLR4, hTLR1/2, hTLR2/6, hTLR5, hTLR7, and hTLR9 cells, respectively.

WST-1 cell proliferation assay. HEK-Blue TLR8 cells were prepared as described above for SEAP reporter assay. After 100 µL of supernatant was removed, a 1:10 dilution of WST-1 reagent (Roche) was added to the cells. Cells were incubated at 37 °C until a color change was observed (30 min–1.5 h). Absorbance was read in a Beckman-Coulter DTX 880 Multimode Detector at 450 nm. Data was normalized with the untreated cells control as 100% survival.

Enzyme-linked immunosorbent assay (ELISA). ELISA was performed to measure TNF-α expression levels. THP-1 cells with phorbol-12-myristate-13-acetate (PMA; 100 ng/mL) treatment were seeded at 2×10^6 per well in 2 mL supplemented RPMI medium (10% (v/v) FBS, 2 mM L-glutamine, 100 µg/mL streptomycin and 100 U/mL penicillin and 0.05 mM 2-mercaptoethanol) in

6-well plates and incubated at 37 °C in a humidified 5% CO₂ atmosphere. After 24 h, the cells were adhered to the surface of the dish. The medium was replaced with unsupplemented RPMI, and the cells were treated with R848 (1 µg/mL) and various concentrations of compounds or left untreated. After 24 h, supernatants of the culture media were collected, and the levels of TNF-α were determined using human TNF-α OptEIA ELISA kit (BD Biosciences) according to the manufacturer's instructions.

RT-PCR analysis of IL-8 and TNF-α mRNA expression. HEK-Blue TLR8 cells were seeded at a density of 1×10^6 cells per well in a 6-well plate. After 24 h incubation, the medium was replaced by serum-free medium, and then the cells were then either left untreated or treated with R848 (1 µg/mL) and various concentrations of compound for 24 h at 37 °C. Then, cells were scraped and resuspended in PBS. RNA was extracted using the E.Z.N.A. total RNA Kit (OMEGA). Reverse transcription was performed using the Qiagen RT First Strand Kit per the manufacturer's instructions using a Bio-Rad T100 thermal cycler. qPCR was performed using SsoAdvanced SYBR Green Supermix from Bio-Rad. RT² qPCR IL-8 and TNF-α primers were obtained from Qiagen. GAPDH primers were obtained from SABiosciences. Data was analyzed using the $\Delta\Delta C_t$ method with GAPDH gene as a housekeeping gene, normalized to time at 0 h.

Protein expression, purification and crystallization. The extracellular domain of human Toll-like receptor 8 (hTLR8, residues 27–827) was prepared as described previously²³, and was concentrated to 16 mg/mL in 10 mM Tris-HCl pH 8.0 and 150 mM NaCl. The protein solutions for the co-crystallization of hTLR8 and inhibitors contained hTLR8 (7.0 mg/mL) and a five-fold excess of inhibitors in a crystallization buffer containing 10 mM Tris-HCl pH 8.0, 150 mM NaCl, and 5% dimethyl sulfoxide (DMSO). Crystallization experiments were performed using sitting-drop vapor-diffusion methods at 293 K. Crystals of hTLR8-CU-CPT were obtained with reservoir solutions containing 12.5% PEG 4000, 0.2 M calcium chloride, 0.1 M Tris-HCl pH 8.0, and 20% ethylene glycol.

Data collection and structure determination. Diffraction data set was collected on beamline PF-AR NE3A (Ibaraki, Japan), PF BL-5A (Ibaraki, Japan), and SPring-8 BL41XU (Hyogo, Japan) under cryogenic conditions at 100 K. The wavelength was set to 1.0000 Å. The data set was processed using the HKL2000 package⁵⁰ or iMOSFM⁵¹. hTLR8-CU-CPT structures were determined by the molecular replacement method using the MOLREP program⁵² with the unliganded hTLR8 structure (PDB ID: 3W3G) as a search model. The model was further refined with stepwise cycles of manual model building using the COOT program⁵³ and restrained refinement using REFMAC⁵⁴ until the R factor was converged. CU-CPT compounds, N-glycans, and water molecules were modeled into the electron density maps at the latter cycles of the refinement. The quality of the final structure was validated with the PDB validation server (<http://wwpdb-validation.wwpdb.org/>). The favored and the allowed regions in the Ramachandran plot were 94% and 6%, respectively, for TLR8-CU-CPT8m, and 94% and 5%, respectively, for TLR8-CU-CPT9b. The statistics of the data collection and refinement are summarized in **Supplementary Table 4**. The figures representing structures were prepared with PyMOL (<http://www.pymol.org>) or CueMol (<http://www.cuemol.org>). Coordinates and structure factor have been deposited in the Protein Data Bank with PDB ID 5WYX (TLR8-CU-CPT8m), and 5WYZ (TLR8-CU-CPT9b).

Isothermal titration calorimetry (ITC). ITC experiments were done in a buffer composed of 25 mM MES pH 5.5, 0.20 M NaCl, and 2.5% DMSO at 298 K using a MicroCal iTC200 (GE Healthcare). The titration sequence included a single 0.4 µL injection followed by 18 injections, 2 µL each, with a spacing of 120 s between the injections. The titration conditions were as follows: 100 µM inhibitors into 10 µM hTLR8; 100 µM R848 into 10 µM hTLR8 and 50 µM inhibitors. OriginLab software (GE Healthcare) was used to analyze the raw ITC data.

Gel filtration chromatography. Gel filtration chromatography experiments were done in a buffer composed of 25 mM MES-NaOH pH 5.5, 0.20 M

NaCl, and 5% DMSO using a Superdex 200 Increase 5/150 GL column (GE Healthcare). For the dose-dependent dimerization of TLR8, the samples (total volume, 25 μ L) containing 1 μ M TLR8 with or without 0.5, 1, 2, 5 μ M (R848 or CU-CPT9b) and 10 μ M (R848 only) were injected. For the concentration-dependent dimerization of TLR8, the samples (total volume, 50 μ L) containing 0.025, 0.05, 0.15, 0.5, 1.5, 5, and 7.5 nmol TLR8; 0.025, 0.5, 0.10, 0.15, 0.25, and 0.50 nmol TLR8 with R848 (TLR8:R848 = 1:5), 0.015, 0.020, 0.025, 0.05, and 0.1 nmol TLR8 with CU-CPT9b (TLR8:CU-CPT9b = 1:5) were injected. Curve-fitting analysis was conducted using ImageJ.

Immunoblotting. Western blot analysis was performed in THP-1 and HEK-Blue TLR8 cells treated with R848 and CU-CPT9a to determine the upregulation/inhibition of phosphorylated-IRAK4 (p-IRAK4), IRAK4, TRAF3 and translocation of p65 component of NF- κ B from cytoplasm to nucleus. THP-1 cells were treated as described above (see “Enzyme-linked immunosorbent assay”). THP-1 cells were collected and lysed, total protein was fractionated into cytoplasmic/nuclear fraction by using NE-PER Nuclear and Cytoplasmic Extraction kit (Thermo Fisher Scientific) according to the manufacturer’s instructions. Protein concentrations were measured by Bradford assay and loaded into 10% Tris-glycine SDS-PAGE. Protein was transferred onto a nitrocellulose membrane (Bio-Rad) or PVDF Transfer membrane (Merck Millipore) by electroblotting (100 mA for 1 h) and probed with the primary antibody IRAK-4 (CST; 4363), p-IRAK4 (CST; 11927), TRAF3 (CST; 4729), IRF3 (CST; 11904), TRIF (CST; 4596) and p65 (CST; 8242) (1:1,000). Peroxidase-conjugated AffiniPure Goat Anti-Rabbit IgG (H+L) antibody (for IRAK-4, p-IRAK4, TRAF3; Huaxingbio; HX2031) at 1:5,000 dilution or peroxidase-conjugated AffiniPure Goat Anti-Rabbit IgG (H+L) antibody (Jackson Immuno Research; 111-035-144; for IRF3, TRIF and p65) at 1:10,000 dilution were used as secondary antibody. 5% w/v BSA in TBST was used for blocking the membrane, and primary, secondary antibody preparation steps. Visualization of the blots was performed by Thermo SuperSignal West Pico kit (Thermo Fisher Scientific) or by Immobilon Western (Millipore). β -actin (CST; 4970), GAPDH (CST; 2118) and lamin A/C (CST; 2032) were used as internal controls for cytosolic and nuclear fractions, respectively.

Tests in human specimens. Human whole blood was collected by venipuncture from healthy human volunteers, rheumatoid arthritis patients, adult-onset Still’s disease (AOSD) patients, and synovial tissue during joint replacement operation for osteoarthritis patients, with informed consent under Institution Review Board (IRB) of Peking Union Medical College Hospital (PUMCH)-approved protocol. All experiments performed on human PBMC and synovial cells have been described and approved by the IRB of PUMCH (No. S-478) and are consistent with Institutional Guidelines. The samples were de-identified after PBMC and synovial cell preparations were made, and the operator who performed the experiments worked with de-identified samples. Diagnosis of rheumatoid arthritis (RA) was confirmed by senior consultant rheumatologists according to 2010 American College of Rheumatology (ACR) criteria for RA. Diagnosis of AOSD was confirmed by a senior consultant rheumatologist according to 1992 ACR criteria, excluding infection, malignancy, and other rheumatic diseases. Diagnosis of osteoarthritis (OA) was confirmed by a senior consultant rheumatologist according to 1995 ACR criteria.

Synovial tissues were derived from patients undergoing joint replacement surgery. Cells were isolated from the synovial membrane⁵⁵. Immediately after separation, cells were cultured at the density of 1×10^6 cells/mL in 0.5 mL of RPMI 1640 in 24-well plates (Thermo Scientific). After 24 h, cells were treated with 0, 10, 20, 40, and 80 μ M of CU-CPT8m. Cells treated with chloroquine (Bide Pharmatech Ltd.) were used as the positive control. After 24 h,

the supernatant was collected and centrifuged for 20 min at 13.2 K r.p.m. at 4 $^{\circ}$ C. The samples were frozen at -80° C until ready for TNF- α measurement. The remaining cells were washed with PBS three times and lysed with lysis buffer (90 μ L 0.5 M EDTA, 9 mL Mammalian Protein Extraction Reagent, 270 μ L NaCl (5 M, aqueous), 90 μ L Halt Protease Inhibitor Single-Use Cocktail, EDTA-free (100 \times)). After 10 min, the mixture was transferred into the corresponding tube, then centrifuged for 20 min at 13.2 K r.p.m. in 4 $^{\circ}$ C. The supernatant was collected into new tubes and frozen at -80° C until ready for interleukin-1 β (IL-1 β) cytokine measurement.

Human PBMCs from four RA patients and one OASD patient were isolated using Density Gradient Centrifugation⁵⁶. Immediately after separation, cells were cultured at a density of 3×10^6 cells/mL in 0.2 mL of RPMI 1640 in 96-well round-bottom plates (Thermo Scientific). Cells were then treated with 0, 10, 40, and 80 μ M of CU-CPT8m or 0, 2.5, 10, 20, and 40 μ M of CU-CPT9a. 6 was used as negative control. Cells treated with 20 μ M chloroquine (Bide Pharmatech Ltd.) were used as the positive control. After incubating for 24 h, the supernatants were collected after centrifuged for 10 min at 4,000 r.p.m. at 4 $^{\circ}$ C and frozen at -80° C until ready for TNF- α measurement.

Statistical analysis. Statistical differences were performed using one-way ANOVA with Bonferroni post-test for multiple comparisons. All statistical analyses were performed using OriginPro 8 for windows, GraphPad Prism, version 6.0 for Mac; a *P* value of <0.05 was considered statistically significant.

Life sciences reporting summary. Further information on experimental design and reagents is available in the **Life Sciences Reporting Summary**.

Data availability. The final atomic coordinates and experimental structure factors were deposited in the Protein Data Bank with accession codes 5WYX and 5WYZ for the TLR8-CU-CPT8m complex, and the TLR8-CU-CPT9b complex structures, respectively. All other data supporting the findings of this study are available within the paper and its supplementary information files.

47. Cheng, K. *et al.* Specific activation of the TLR1-TLR2 heterodimer by small-molecule agonists. *Sci. Adv.* **1**, e1400139 (2015).
48. Csakai, A. *et al.* Saccharin derivatives as inhibitors of interferon-mediated inflammation. *J. Med. Chem.* **57**, 5348–5355 (2014).
49. Das, N. *et al.* HMGB1 activates proinflammatory signaling via TLR5 leading to allodynia. *Cell Rep.* **17**, 1128–1140 (2016).
50. Otwinowski, Z. & Minor, W. Processing of X-ray diffraction data collected in oscillation mode. *Methods Enzymol.* **276**, 307–326 (1997).
51. Batty, T.G., Kontogiannis, L., Johnson, O., Powell, H.R. & Leslie, A.G. iMOSFLM: a new graphical interface for diffraction-image processing with MOSFLM. *Acta Crystallogr. D Biol. Crystallogr.* **67**, 271–281 (2011).
52. Vagin, A. & Teplyakov, A. Molecular replacement with MOLREP. *Acta Crystallogr. D Biol. Crystallogr.* **66**, 22–25 (2010).
53. Emsley, P. & Cowtan, K. Coot: model-building tools for molecular graphics. *Acta Crystallogr. D Biol. Crystallogr.* **60**, 2126–2132 (2004).
54. Murshudov, G.N., Vagin, A.A. & Dodson, E.J. Refinement of macromolecular structures by the maximum-likelihood method. *Acta Crystallogr. D Biol. Crystallogr.* **53**, 240–255 (1997).
55. Brennan, F.M., Chantry, D., Jackson, A.M., Maini, R.N. & Feldmann, M. Cytokine production in culture by cells isolated from the synovial membrane. *J. Autoimmun.* **2** (Suppl.) 177–186 (1989).
56. Ulmer, A.J., Scholz, W., Ernst, M., Brandt, E. & Flad, H.D. Isolation and subfractionation of human peripheral blood mononuclear cells (PBMC) by density gradient centrifugation on Percoll. *Immunobiology* **166**, 238–250 (1984).

Life Sciences Reporting Summary

Nature Research wishes to improve the reproducibility of the work that we publish. This form is intended for publication with all accepted life science papers and provides structure for consistency and transparency in reporting. Every life science submission will use this form; some list items might not apply to an individual manuscript, but all fields must be completed for clarity.

For further information on the points included in this form, see [Reporting Life Sciences Research](#). For further information on Nature Research policies, including our [data availability policy](#), see [Authors & Referees](#) and the [Editorial Policy Checklist](#).

▶ Experimental design

1. Sample size

Describe how sample size was determined.

We chose the sample size based on literatures in the field.

2. Data exclusions

Describe any data exclusions.

Not excluded

3. Replication

Describe whether the experimental findings were reliably reproduced.

Yes

4. Randomization

Describe how samples/organisms/participants were allocated into experimental groups.

No randomization

5. Blinding

Describe whether the investigators were blinded to group allocation during data collection and/or analysis.

No blinding

Note: all studies involving animals and/or human research participants must disclose whether blinding and randomization were used.

6. Statistical parameters

For all figures and tables that use statistical methods, confirm that the following items are present in relevant figure legends (or in the Methods section if additional space is needed).

n/a Confirmed

- The exact sample size (n) for each experimental group/condition, given as a discrete number and unit of measurement (animals, litters, cultures, etc.)
- A description of how samples were collected, noting whether measurements were taken from distinct samples or whether the same sample was measured repeatedly
- A statement indicating how many times each experiment was replicated
- The statistical test(s) used and whether they are one- or two-sided (note: only common tests should be described solely by name; more complex techniques should be described in the Methods section)
- A description of any assumptions or corrections, such as an adjustment for multiple comparisons
- The test results (e.g. P values) given as exact values whenever possible and with confidence intervals noted
- A clear description of statistics including central tendency (e.g. median, mean) and variation (e.g. standard deviation, interquartile range)
- Clearly defined error bars

See the web collection on [statistics for biologists](#) for further resources and guidance.

► Software

Policy information about [availability of computer code](#)

7. Software

Describe the software used to analyze the data in this study.

GraphPad Prism, Origin Pro

For manuscripts utilizing custom algorithms or software that are central to the paper but not yet described in the published literature, software must be made available to editors and reviewers upon request. We strongly encourage code deposition in a community repository (e.g. GitHub). *Nature Methods* [guidance for providing algorithms and software for publication](#) provides further information on this topic.

► Materials and reagents

Policy information about [availability of materials](#)

8. Materials availability

Indicate whether there are restrictions on availability of unique materials or if these materials are only available for distribution by a for-profit company.

There are no restrictions on availability upon request of materials for researchers, scholars and lay persons expressing legitimate interest in the studies.

9. Antibodies

Describe the antibodies used and how they were validated for use in the system under study (i.e. assay and species).

Described in methods "Confocal imaging" and "Immunoblotting".

10. Eukaryotic cell lines

a. State the source of each eukaryotic cell line used.

Described in methods "Confocal imaging" and "Immunoblotting".

b. Describe the method of cell line authentication used.

N/A

c. Report whether the cell lines were tested for mycoplasma contamination.

Yes, described in methods "Cell culture".

d. If any of the cell lines used are listed in the database of commonly misidentified cell lines maintained by [ICLAC](#), provide a scientific rationale for their use.

N/A

► Animals and human research participants

Policy information about [studies involving animals](#); when reporting animal research, follow the [ARRIVE guidelines](#)

11. Description of research animals

Provide details on animals and/or animal-derived materials used in the study.

N/A

Policy information about [studies involving human research participants](#)

12. Description of human research participants

Describe the covariate-relevant population characteristics of the human research participants.

Described in methods "Test in human specimens".